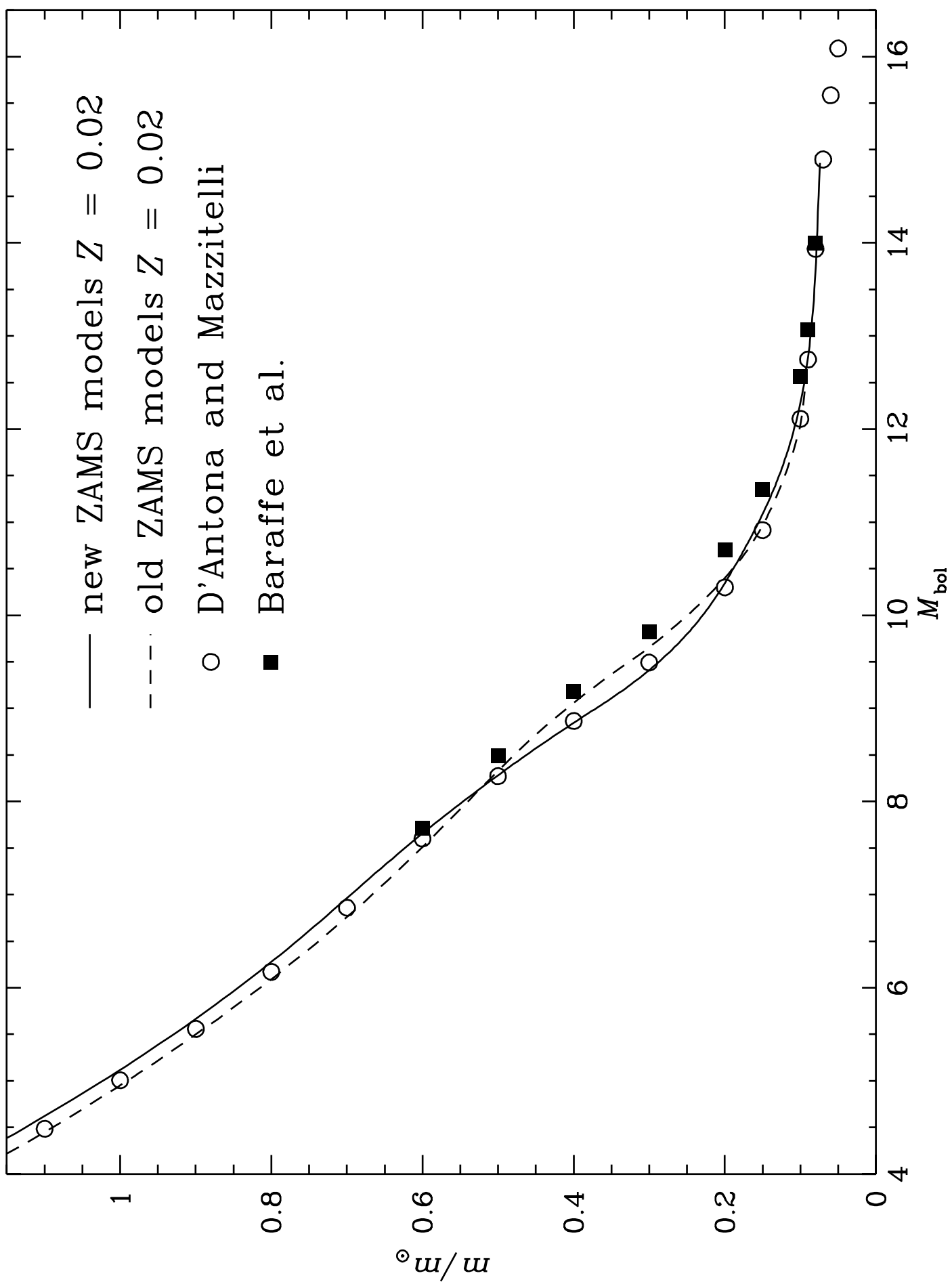


## APPENDIX

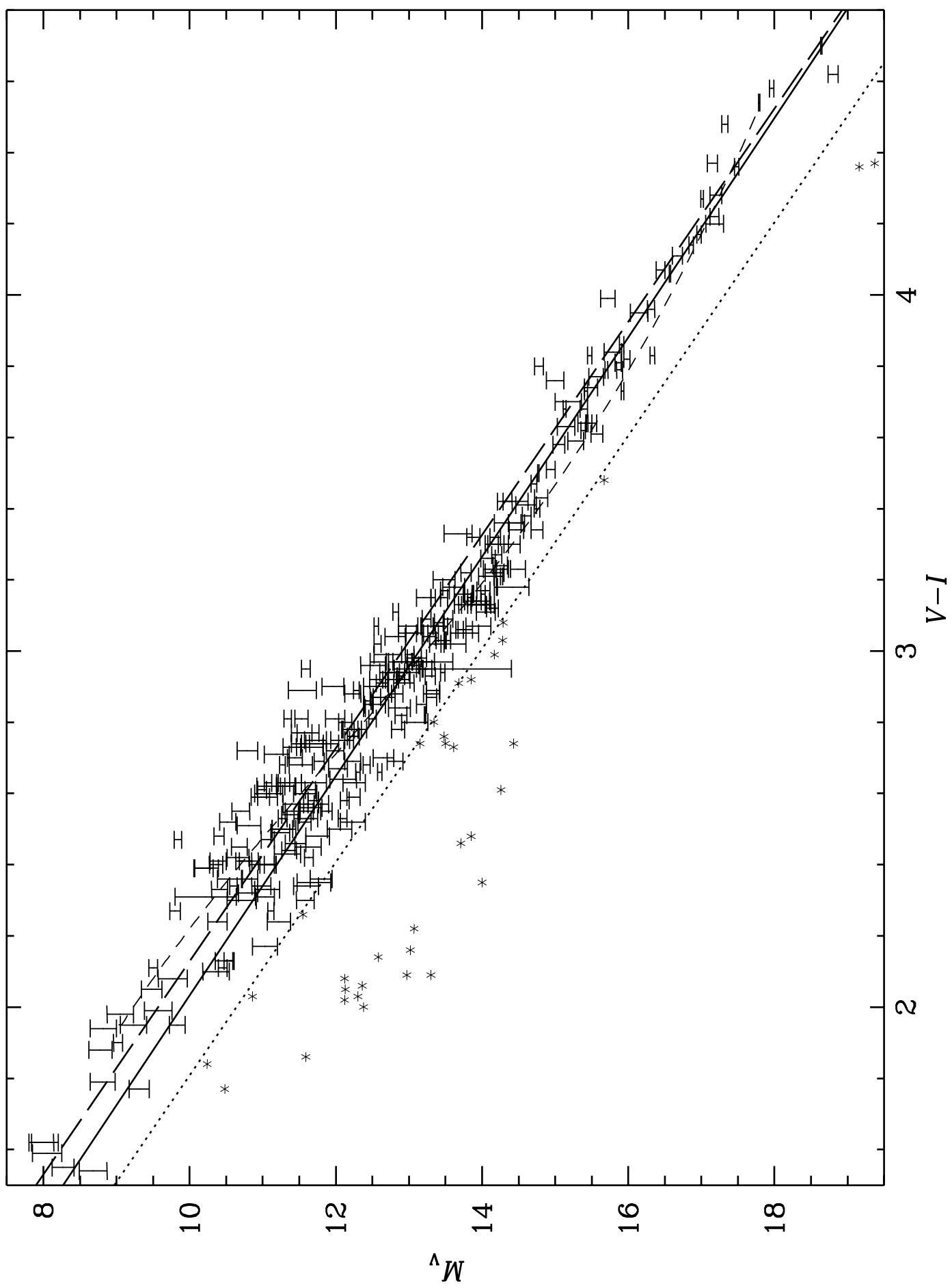
**Table A.** Derivatives of the empirical mass-luminosity relation.

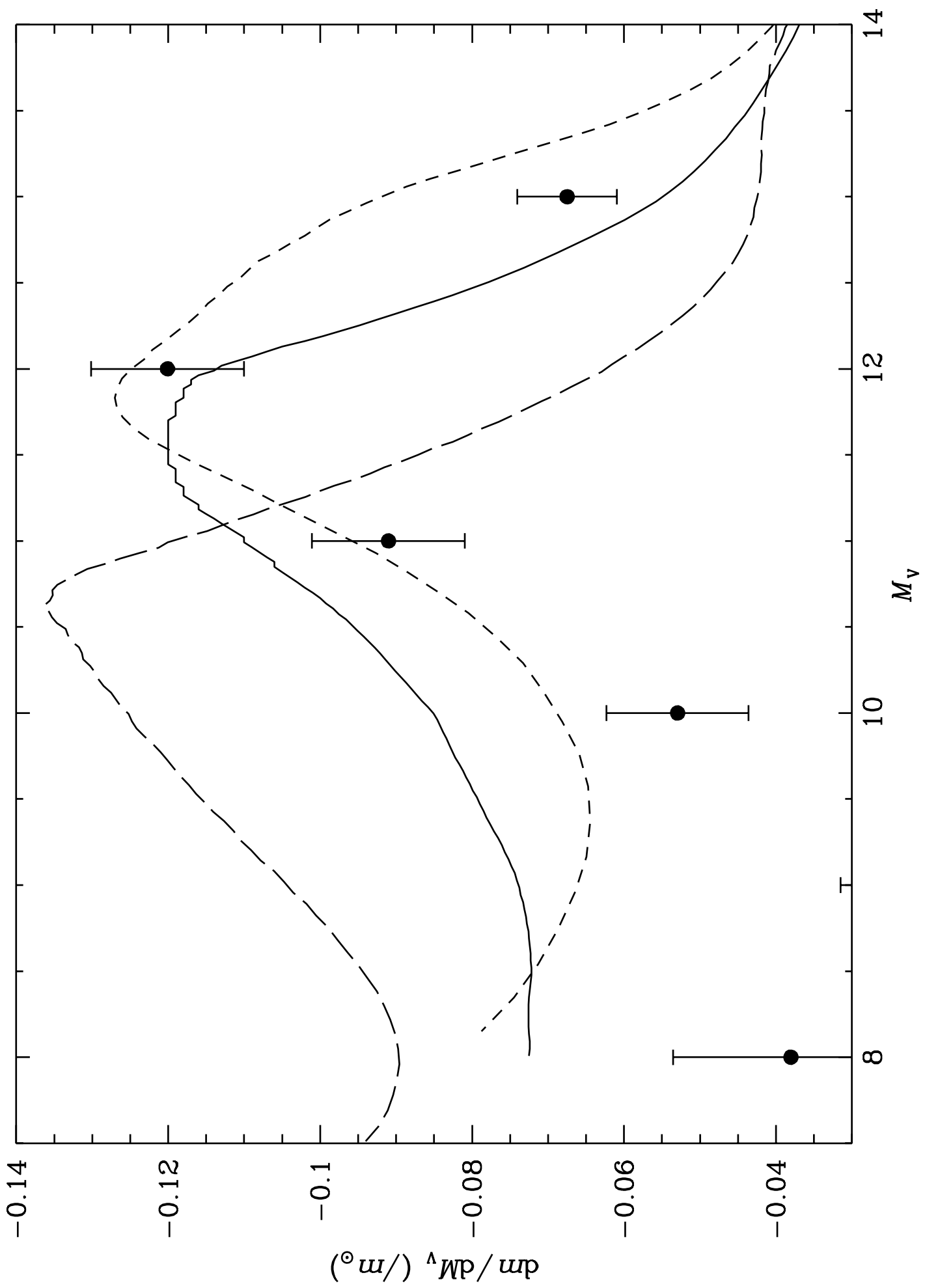
In the table we list our (Kroupa, Tout & Gilmore 1993) empirical mass–luminosity relation in bolometric magnitudes and various photometric pass bands as a function of mass, together with the derivatives of mass with respect to each magnitude. Masses are in units of the solar mass. Derivatives have been multiplied by 10. Details can be found in Section 3.2.

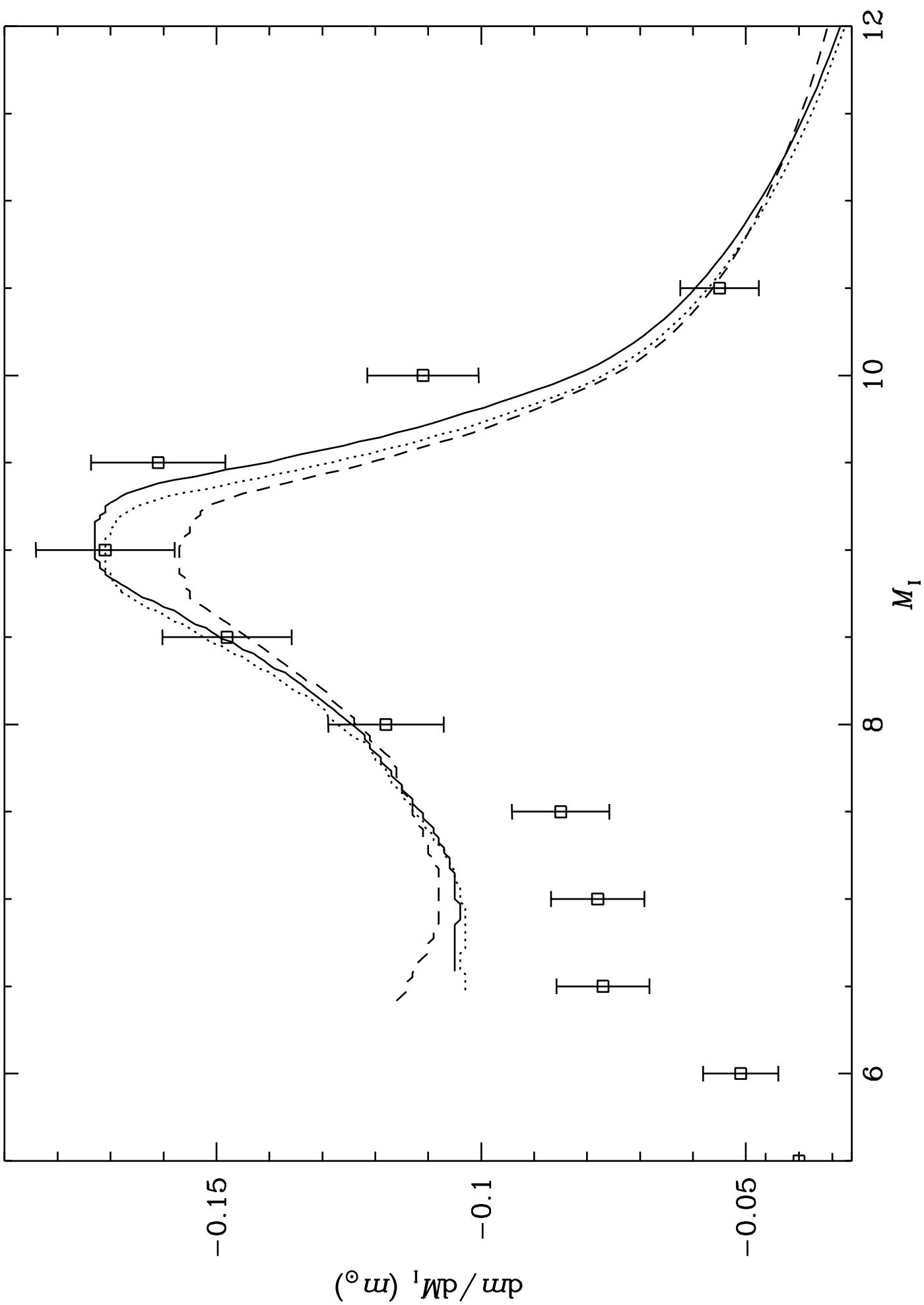
$m$	$M_{\text{bol}}$	$\frac{dm}{dM_{\text{bol}}}$	$M_V$	$\frac{dm}{dM_V}$	$M_I$	$\frac{dm}{dM_I}$	$M_J$	$\frac{dm}{dM_J}$	$M_H$	$\frac{dm}{dM_H}$	$M_K$	$\frac{dm}{dM_K}$
0.650	7.086	-0.993	8.008	-0.725	6.587	-1.050	5.507	-1.420	4.896	-1.480	4.747	-1.610
0.635	7.241	-1.000	8.221	-0.726	6.735	-1.050	5.617	-1.390	5.002	-1.440	4.845	-1.560
0.619	7.395	-1.010	8.434	-0.723	6.882	-1.040	5.731	-1.340	5.112	-1.380	4.946	-1.500
0.604	7.547	-1.020	8.647	-0.724	7.030	-1.050	5.847	-1.310	5.225	-1.340	5.051	-1.440
0.588	7.698	-1.030	8.859	-0.731	7.177	-1.060	5.966	-1.290	5.342	-1.310	5.159	-1.410
0.573	7.845	-1.060	9.069	-0.744	7.322	-1.080	6.086	-1.280	5.461	-1.290	5.270	-1.380
0.558	7.988	-1.100	9.273	-0.766	7.463	-1.110	6.206	-1.290	5.580	-1.290	5.382	-1.370
0.542	8.126	-1.140	9.471	-0.790	7.600	-1.140	6.325	-1.300	5.699	-1.290	5.495	-1.370
0.527	8.258	-1.190	9.664	-0.812	7.734	-1.170	6.443	-1.320	5.819	-1.300	5.607	-1.370
0.511	8.386	-1.230	9.851	-0.834	7.863	-1.210	6.559	-1.330	5.937	-1.300	5.720	-1.360
0.496	8.509	-1.270	10.034	-0.858	7.990	-1.240	6.675	-1.350	6.056	-1.310	5.834	-1.360
0.480	8.628	-1.340	10.210	-0.894	8.112	-1.290	6.788	-1.390	6.172	-1.340	5.946	-1.390
0.465	8.741	-1.400	10.380	-0.928	8.229	-1.340	6.898	-1.420	6.286	-1.370	6.056	-1.410
0.450	8.849	-1.460	10.543	-0.966	8.342	-1.400	7.004	-1.470	6.398	-1.410	6.164	-1.440
0.434	8.952	-1.540	10.699	-1.010	8.450	-1.460	7.107	-1.530	6.505	-1.460	6.269	-1.490
0.419	9.049	-1.620	10.848	-1.060	8.553	-1.520	7.206	-1.590	6.610	-1.510	6.371	-1.540
0.403	9.143	-1.690	10.992	-1.100	8.652	-1.580	7.302	-1.650	6.710	-1.560	6.470	-1.590
0.388	9.232	-1.770	11.130	-1.140	8.748	-1.650	7.394	-1.710	6.807	-1.620	6.566	-1.640
0.372	9.317	-1.840	11.263	-1.180	8.840	-1.700	7.482	-1.760	6.901	-1.670	6.658	-1.690
0.357	9.400	-1.870	11.393	-1.190	8.930	-1.720	7.569	-1.790	6.992	-1.700	6.749	-1.710
0.342	9.482	-1.890	11.522	-1.200	9.019	-1.730	7.655	-1.810	7.083	-1.710	6.838	-1.730
0.326	9.564	-1.900	11.650	-1.200	9.108	-1.730	7.740	-1.810	7.173	-1.720	6.927	-1.740
0.311	9.645	-1.900	11.779	-1.190	9.197	-1.720	7.825	-1.810	7.263	-1.720	7.016	-1.730
0.295	9.726	-1.880	11.910	-1.170	9.288	-1.690	7.911	-1.790	7.353	-1.710	7.105	-1.720
0.280	9.810	-1.800	12.044	-1.110	9.381	-1.610	7.998	-1.710	7.445	-1.630	7.196	-1.650
0.264	9.900	-1.620	12.191	-0.996	9.482	-1.440	8.093	-1.550	7.544	-1.480	7.294	-1.500
0.249	10.001	-1.430	12.356	-0.875	9.596	-1.260	8.198	-1.380	7.654	-1.330	7.402	-1.350
0.234	10.117	-1.250	12.546	-0.755	9.728	-1.090	8.318	-1.210	7.778	-1.170	7.524	-1.190
0.218	10.250	-1.070	12.767	-0.644	9.881	-0.931	8.455	-1.050	7.919	-1.020	7.662	-1.050
0.203	10.406	-0.912	13.029	-0.540	10.062	-0.780	8.613	-0.905	8.081	-0.890	7.820	-0.916
0.187	10.587	-0.799	13.337	-0.466	10.275	-0.674	8.794	-0.809	8.264	-0.804	7.997	-0.832
0.172	10.792	-0.711	13.692	-0.408	10.521	-0.590	8.994	-0.738	8.464	-0.742	8.190	-0.774
0.156	11.022	-0.636	14.095	-0.358	10.800	-0.517	9.212	-0.680	8.679	-0.692	8.396	-0.727
0.141	11.278	-0.568	14.557	-0.312	11.119	-0.451	9.448	-0.629	8.910	-0.648	8.614	-0.685
0.126	11.567	-0.504	15.088	-0.270	11.487	-0.390	9.703	-0.580	9.156	-0.605	8.846	-0.645
0.110	11.893	-0.443	15.707	-0.230	11.916	-0.332	9.981	-0.532	9.421	-0.561	9.094	-0.602
0.095	12.267	-0.383	16.444	-0.191	12.425	-0.275	10.285	-0.481	9.708	-0.512	9.361	-0.553
0.079	12.706	-0.323	17.347	-0.153	13.050	-0.221	10.626	-0.425	10.026	-0.457	9.655	-0.495

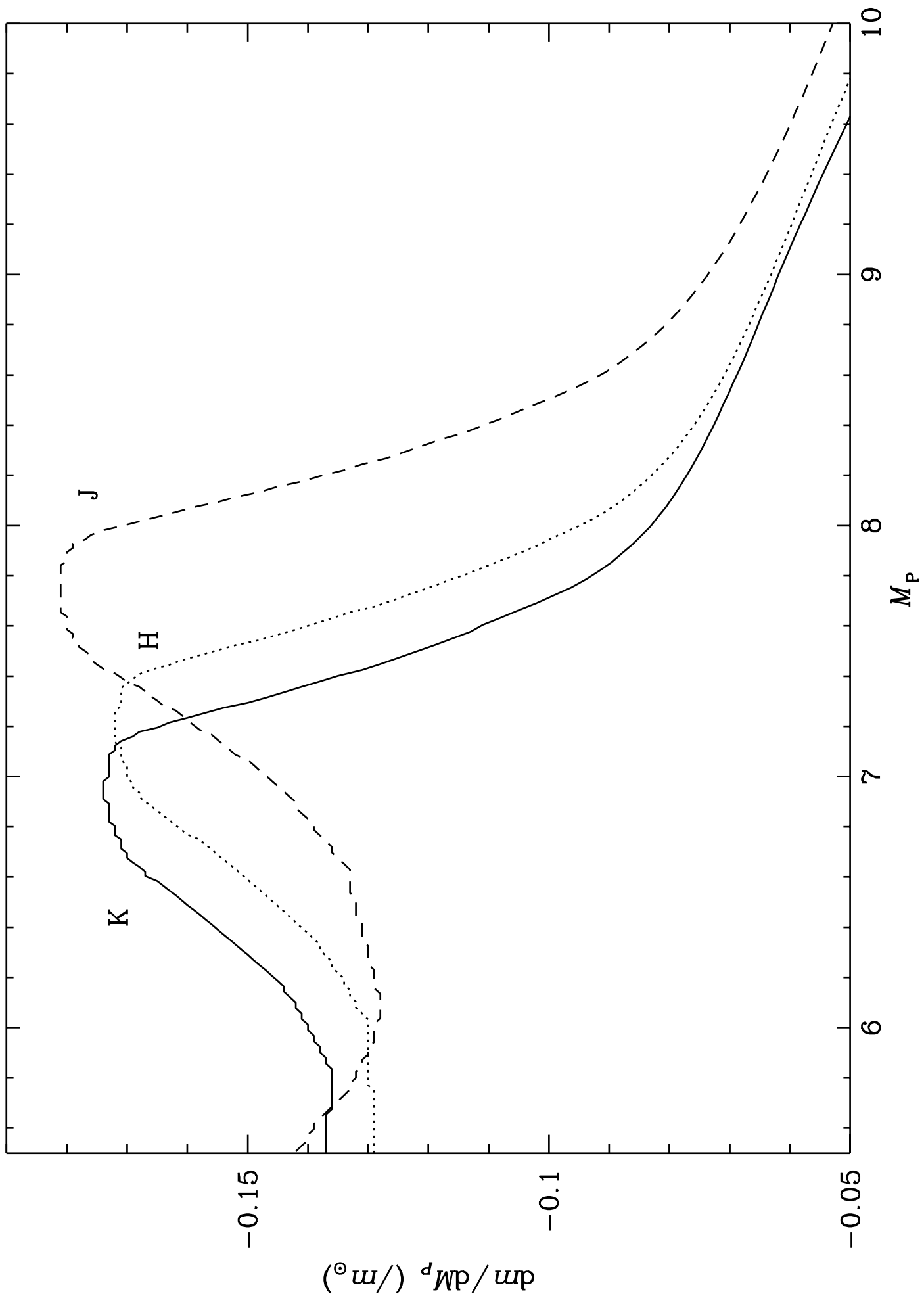


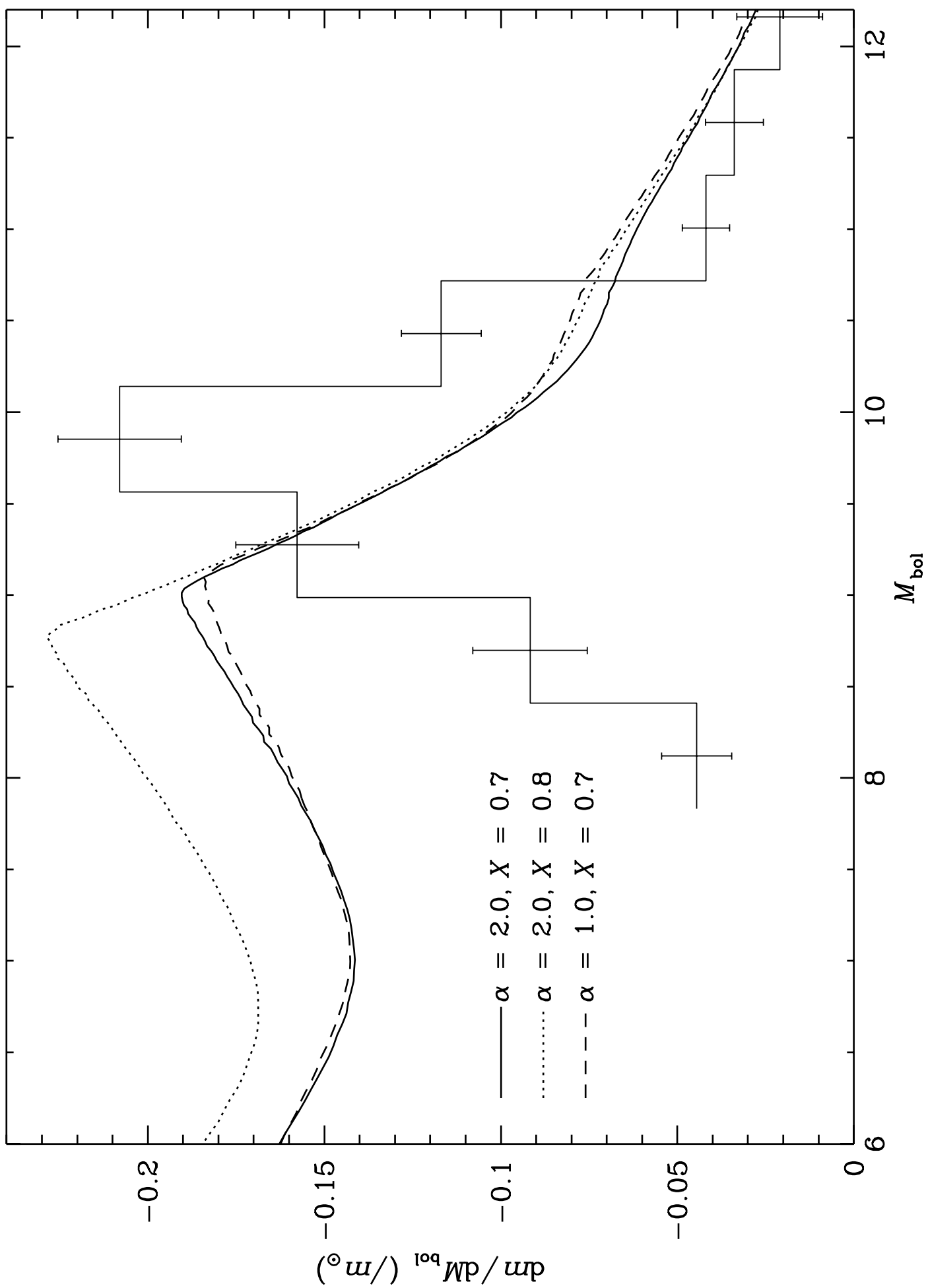


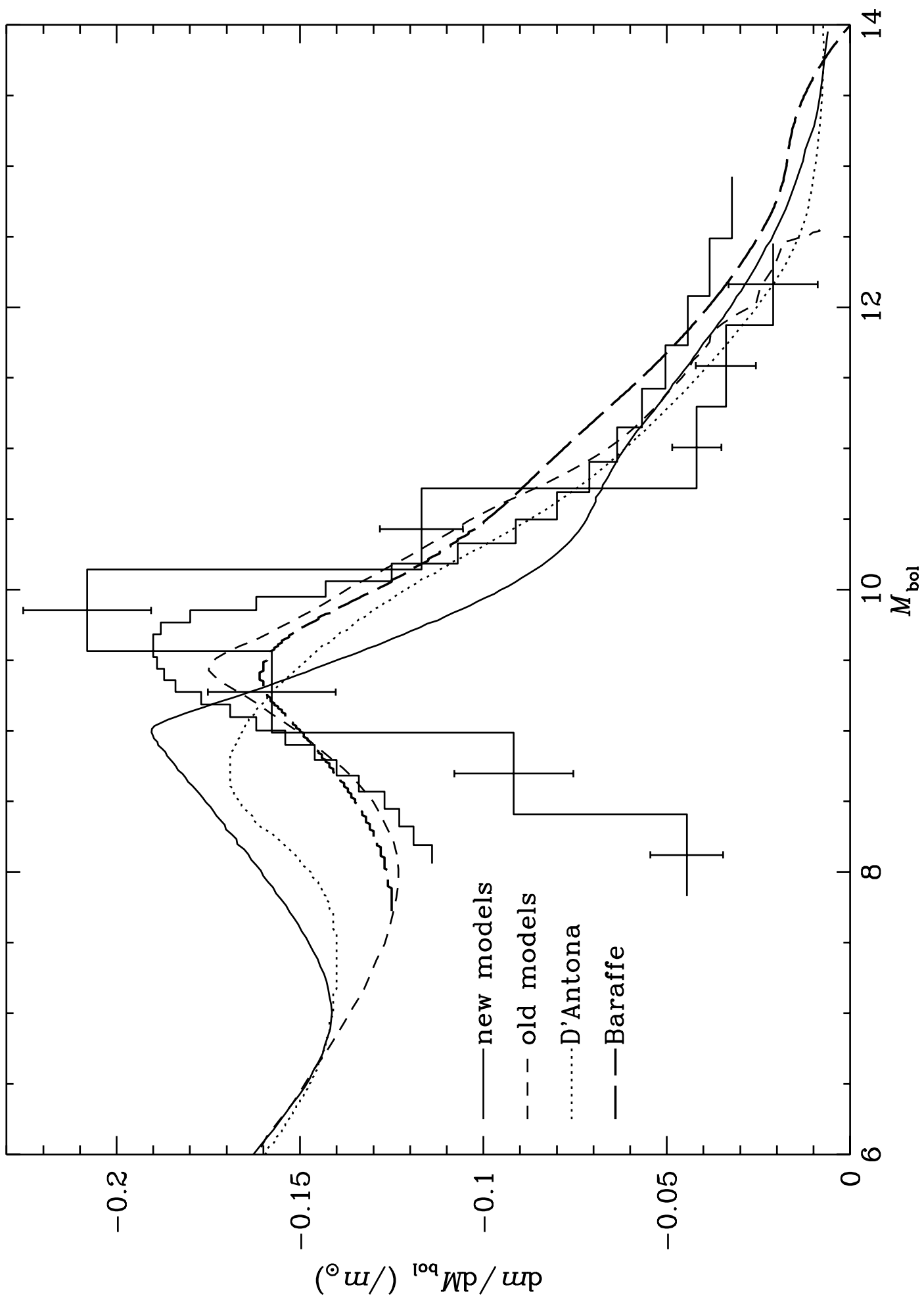


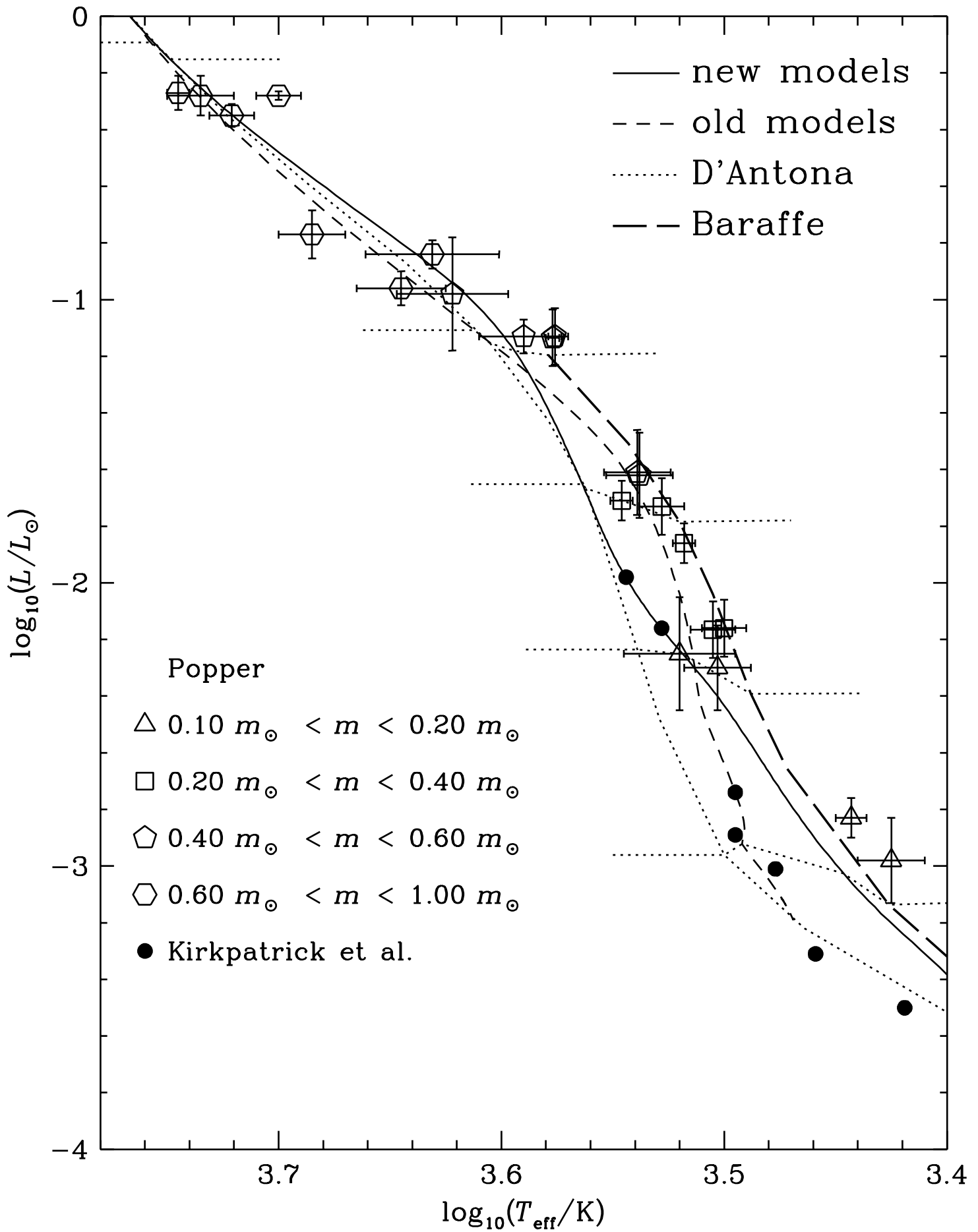


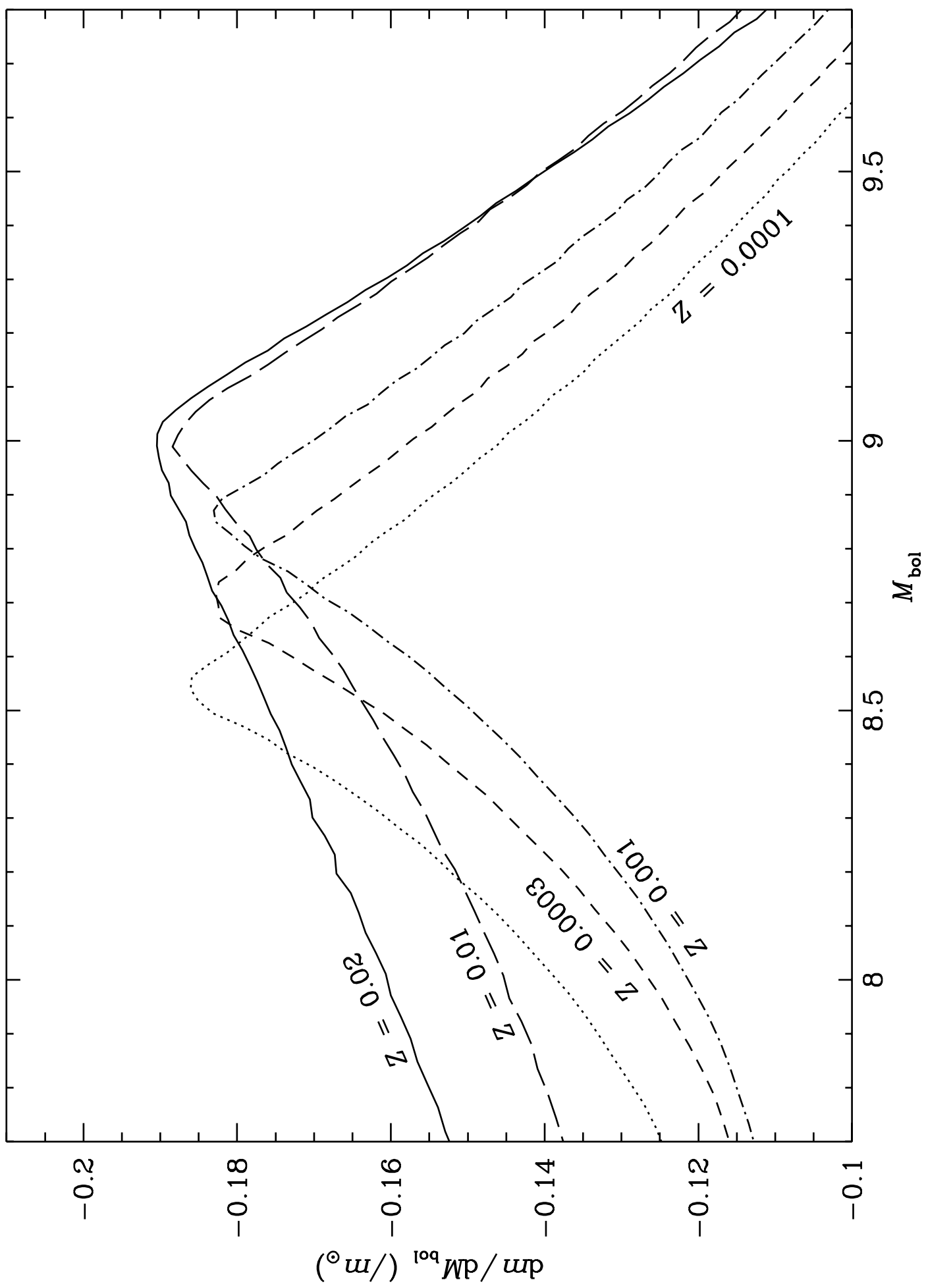


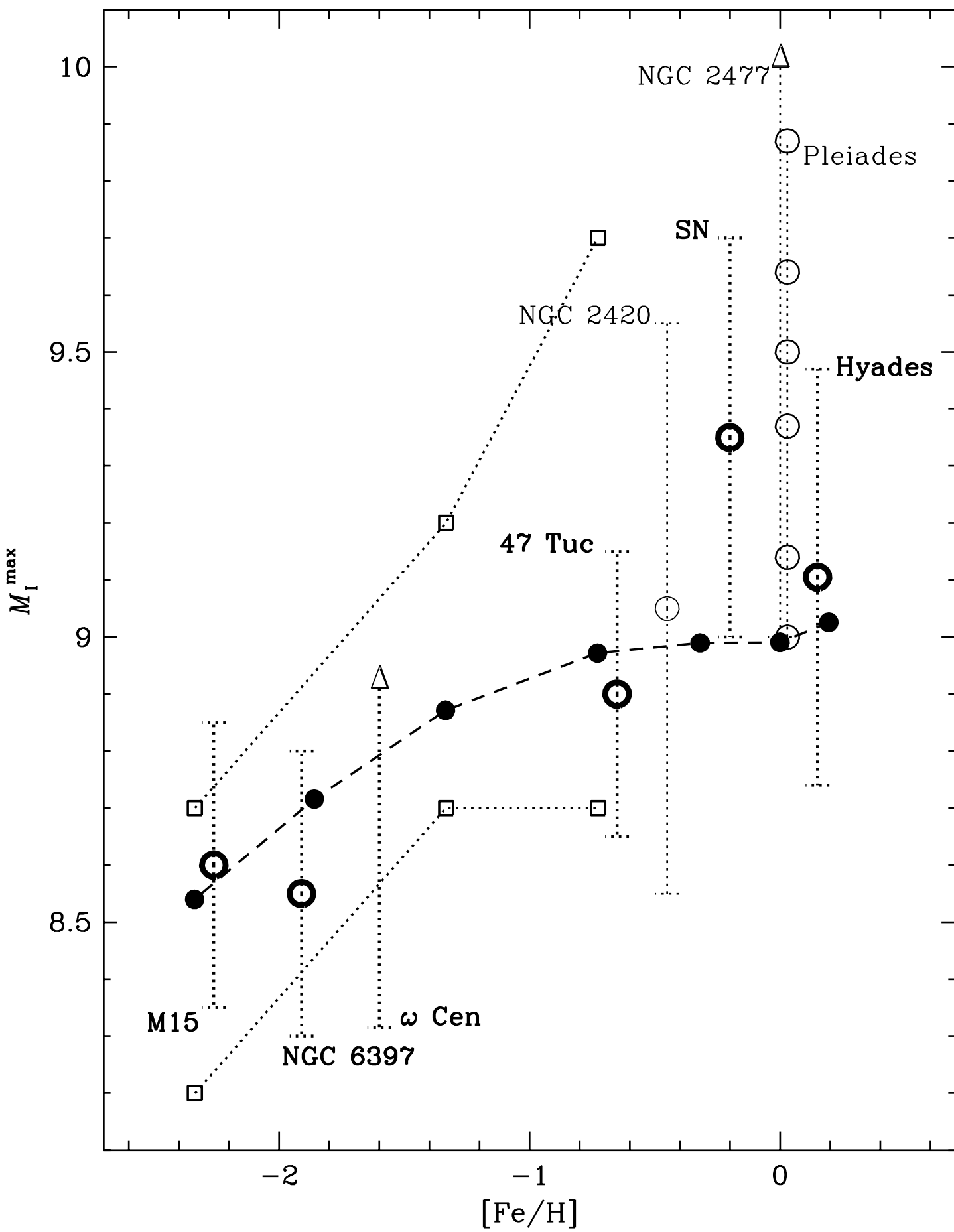












The Theoretical Mass–Magnitude Relation of Low-Mass Stars  
and its Metallicity Dependence

Pavel Kroupa<sup>1</sup> and Christopher A. Tout<sup>2,3,4</sup>

<sup>1</sup>Astronomisches Rechen-Institut  
Mönchhofstraße 12-14, D-69120 Heidelberg, Germany  
e-mail: s48@ix.urz.uni-heidelberg.de

<sup>2</sup>Space Telescope Science Institute,  
3700 San Martin drive, Baltimore, MD 21218, U.S.A.  
e-mail: cat@ast.cam.ac.uk

<sup>3</sup>On leave from University of Cambridge

<sup>4</sup>Current Address: Konkoly Observatory of the Hungarian Academy of Sciences,  
H-1525 Budapest, P.O.B. 67, Hungary

MNRAS, in press

**Abstract.** We investigate the dependence of theoretically generated mass–(absolute magnitude) relations on stellar models. Using up-to-date physics we compute models of stars in the mass range  $0.1 < m \leq 1 m_{\odot}$ . We compare the solar-metallicity models with our older models and also with recent models computed by others. We further compare with an empirical mass–(absolute magnitude) relation that best fits the observed data. At a given mass below  $0.6 m_{\odot}$  the effective temperatures differ substantially from model to model. However taken individually each set of models is in good agreement with observations in the mass–luminosity plane. A minimum in the derivative  $dm/dM_V$  at  $M_V \approx 11.5$ , which is due to H<sub>2</sub> formation and establishment of a fully convective stellar interior, is present in all photometric bands, for all models but its position changes from model to model. This minimum leads to a maximum in the stellar luminosity function for Galactic disk stars at  $M_V \approx 11.5$ ,  $M_{\text{bol}} \approx 9.8$ . Precise stellar models should locate this maximum in the stellar luminosity function at the same magnitude as observations. This is an extra constraint on low-mass stellar models. Models which incorporate the most realistic theoretical atmospheres and the most recent equation of state and opacities can satisfy this constraint. These models are also in best agreement with the most recent luminosity–(effective temperature) and mass–luminosity data. Each set of our models of a given metallicity (in the range  $0.2 > [\text{Fe}/\text{H}] > -2.3$ ) shows a maximum in  $-dm/dM_{\text{bol}}$ , which moves to brighter bolometric magnitudes with decreasing metallicity. The change in location of the maximum, as a function of [Fe/H], follows the location of structure in luminosity functions for stellar populations with different metal abundances. This structure seen in all observed stellar populations can be accounted for by the mass–luminosity relation and does not require a maximum in the stellar mass function at  $m \approx 0.3 m_{\odot}$ .

*Subject headings:* stars: low-mass, brown dwarfs – stars: population I and II – stars: luminosity function, mass function – open clusters and associations: general – globular clusters: general

## 1 INTRODUCTION

It is desirable to understand the shape of the luminosity function in terms of the underlying mass function. However, observed luminosity functions depend, not only on the associated mass functions but also rather delicately on the mass-luminosity relation of the stars. This is demonstrated well by Elson et al. (1995, figure 6) and has been stressed before by D'Antona & Mazzitelli (1983) and later by Kroupa, Tout & Gilmore (1990). The unobservable distribution of stellar masses is mapped to the observable distribution of stellar luminosities by multiplying the former by the derivative of the mass-luminosity relation.

D'Antona & Mazzitelli (1994) point out that significant uncertainties remain in our understanding of stellar physics for stars less massive than about  $0.6 m_{\odot}$  because atmospheric convection and opacities are not yet fully understood. Further discussion of the uncertainties in stellar structure theory that result from different treatments of the surface boundary condition is given by Chabrier, Baraffe & Plez (1996). Despite these uncertainties, models of low-mass stars with a fixed chemical composition demonstrate that the absolute magnitude is not a simple linear function of stellar mass because opacities, the equation of state and consequently stellar structure change significantly with mass. The derivative  $dm/dM_V$  varies substantially with absolute visual magnitude  $M_V$ . It has a local maximum at  $M_V \approx 7 - 8$  and a pronounced minimum at  $M_V \approx 11.5$ , for solar metallicity stars (Kroupa, Tout & Gilmore 1990). These features coincide, respectively, with a plateau or depression at  $M_V \approx 7$  and a pronounced maximum at  $M_V \approx 11.5$  observed in the stellar luminosity function. D'Antona & Mazzitelli (1983) noted that the flattening in the luminosity function at  $M_V \approx 6 - 9$  is probably due to the existence of an inflection in the mass-luminosity relation at a mass near  $m = 0.6 m_{\odot}$ . Copeland, Jensen & Jorgensen (1970) constructed stellar models in the mass range  $0.25 - 2.5 M_{\odot}$ , and attributed this increased luminosity near  $m = 0.5 - 0.7 M_{\odot}$  to the onset of H<sub>2</sub> formation in low-mass stars. They showed how the associated increase in effective temperature  $T_{\text{eff}}$  leads to a break in the main sequence in the HR diagram at  $\log_{10}(T_{\text{eff}}/K) \approx 3.6$ . More detailed modelling led Kroupa, Tout & Gilmore (1990) to suggest that this flattening in the luminosity function at  $M_V \approx 7$  ( $m \approx 0.7 m_{\odot}$ ) is caused by increased importance of H<sup>-</sup> opacity in low-mass stars as the stellar mass is reduced, and that the *onset* of H<sub>2</sub> formation in a thin outer shell at  $m \approx 0.5 m_{\odot}$  (their figs. 2 and 3) leads to an increase in  $-dm/dM_V$  with increasing  $M_V$  until a maximum at  $M_V \approx 11.5$  ( $m \approx 0.35 m_{\odot}$ ) is reached, where the stars are also fully convective. They derived an empirical shape for the  $m(M_V)$  relation by comparing the observed luminosity function with smooth mass functions. Recent mass-luminosity data (Henry & McCarthy 1993) is in good agreement with this shape.

If the original assertion by Kroupa, Tout & Gilmore (1990), that the peak in the luminosity function at  $M_V \approx 11.5$  is due to the minimum in  $dm/dM_V$ , is true then similar structure should exist in the luminosity function of different stellar populations, as pointed out by Kroupa, Tout & Gilmore (1993). Further, Kroupa (1995a) stresses that the amplitude and location of the peak in the stellar luminosity function may be used as an additional constraint on stellar models. Indeed observations with the Hubble Space Telescope show that the stellar luminosity functions in the three globular clusters NGC 3697, M15 and 47 Tucanae (Paresce, De Marchi & Romaniello 1995, De Marchi & Paresce 1995a, 1995b, respectively) also have maxima. These lie at luminosities somewhat brighter than the luminosity of the maximum in the solar neighbourhood luminosity function.

Here we investigate both the extra constraint imposed on population I models by the shape of the luminosity function and the sensitivity of the mass-(absolute magnitude) relation to changes in metallicity. Of interest is the slope of the  $m(M_P)$  relation, where  $P$  represents an arbitrary magnitude band, near  $m = 0.35 m_{\odot}$  so we need a fine grid of stellar models in the mass range  $0.1 - 0.5 m_{\odot}$ . We use the latest version of the Eggleton evolution code (Pols et al. 1995; Tout et al. 1996) to compute a new set of low-mass stellar models. The code incorporates substantial recent improvements in our understanding of the physics of stellar interiors, particularly the opacity and the equation of state. We then compare with our computations based on older opacities and equation of state and with models recently computed by others (Baraffe et al. 1995; D'Antona & Mazzitelli 1994).

In Section 2 we introduce the stellar models. They are compared with the observations of Galactic disk stars in Section 3. The implications for the population-II stellar luminosity function are considered in Section 4. In Section 5 we summarise our conclusions.

## 2 STELLAR MODELS

In addition to our own models we consider the work of D'Antona & Mazzitelli (1994) and Baraffe et al. (1995). We need stellar models with masses in the range  $0.1 m_{\odot} \leq m \leq 0.5 m_{\odot}$  so that we can quantify the first derivative of the mass–(absolute magnitude) relation near  $m = 0.35m_{\odot}$ . Although other, commonly used models are to be found in the literature they are not sufficiently well defined for these purposes.

### 2.1 Our New and Old Models

We make our stellar models with the Eggleton evolution code (Eggleton 1971, 1972, 1973). The most recent version of this code is described by Pols et al. (1995). It incorporates new nuclear reaction rates (Caughlan & Fowler 1988) and opacities (Iglesias, Rogers & Wilson 1992, OPAL; Alexander & Ferguson 1994). It also uses a new equation of state (described in detail by Pols et al.) which treats ionization equilibria, including pressure ionization, somewhat more precisely and includes Coulomb interactions. This equation of state fits well with that used by Iglesias, Rogers and Wilson for their opacity computations. The code has been further improved by incorporation of bicubic spline interpolations in opacity (Tout et al. 1996). Our population I models have a metallicity  $Z = 0.02$ , a hydrogen abundance  $X = 0.7$  and a helium abundance  $Y = 0.28$ . We use  $\alpha = 2$  for the mixing length parameter. In the old models the zero-age mixture of metals was determined by the tables of Cox & Stewart (1970) while for the new models we use the Solar system meteoritic mixture determined by Anders & Grevesse (1989). Accurate analytic fits to the new models are given by Tout et al. (1996).

Below we show that these new models do not fit the population I observations as well as the old models computed by Kroupa, Tout & Gilmore (1990) that used Cox & Stewart (1970) opacities, reaction rates from Caughlan, Fowler & Zimmerman (1975) and an equation of state based on that of Eggleton, Faulkner & Flannery (1973), with pressure ionization described by Hjellming (1989) and a simple treatment of hydrogen molecules (Webbink 1975). Both the old and the new models use a simple Eddington approximation (Woolley & Stibbs 1953), rather than a stellar atmosphere calculation, for the surface boundary conditions.

Keeping this in mind, we use the new and old models to illustrate the differences in the HR diagram, in the  $m(M_P)$  and the  $dm/dM_P(M_P)$  planes, that result from changes in the input physics. This allows us some insight into which observational constraint tests which aspect of the input physics. We follow the less established convention of writing mass as a function of magnitude because we are trying to identify the mass of a star with a particular observed magnitude. Also, by computing our own models, we can define a high resolution on the mass grid, which is necessary when studying the derivative of the mass–luminosity relation. We compute 300 stellar models with masses  $0.1 \leq m \leq 1 m_{\odot}$  distributed uniformly in  $\log_{10}m$ .

### 2.2 Models by D'Antona & Mazzitelli

The greatest deficiency in our models lies in our treatment of the surface boundary conditions. This is partially remedied in the work of D'Antona & Mazzitelli (1994, also private communication) who use a grey-body atmosphere integration to an optical depth of  $\tau = 2/3$ . They compute four sets of models using mixing length theory (MLT) or their alternative treatment of convection, and the Alexander (Alexander & Ferguson 1994) or Kurucz (1991) opacities. We consider only the models that have Alexander opacities at low temperatures and MLT, because (i) the Kurucz opacities do not include molecules and (ii) the alternative treatment of convection together with Alexander opacities gives main-sequence stellar models that are virtually indistinguishable from models computed using MLT and Alexander opacities. To ensure arrival on the main sequence we use their  $10^9$  yr isochrone. The models listed in their tables 3 and 7 are spaced by  $0.1 m_{\odot}$  for  $m \geq 0.2 m_{\odot}$ , so that the resolution of the slope of the mass–(bolometric magnitude) relation,  $dm/dM_{\text{bol}}$ , in the critical region around  $0.35 m_{\odot}$  is limited.

### 2.3 Models by Baraffe et al.

Baraffe et al. (1995) substantially improve the atmospheric modelling. They allow for convection to extend into the atmosphere and find that it can indeed reach to an optical depth  $\tau \ll 1$ . Chabrier et al. (1996) discuss the effects of different atmospheric models on stellar modelling. Baraffe et al. tabulate their models in their table 1 with a resolution of  $0.1 m_{\odot}$  in mass, which again limits definition of the maximum in  $-dm/dM_{\text{bol}}$ .

## 3 POPULATION I STARS: COMPARISON WITH OBSERVATIONAL CONSTRAINTS

We can now compare the stellar models introduced in Section 2 with observations in the hope of learning which physics (opacities, equation of state, treatment of the atmosphere) leads to stellar models that are most consistent with available observational constraints.

### 3.1 The mass–(absolute magnitude) relation

Taken alone each set of models is in rather good agreement with observations in the mass–(bolometric magnitude) plane. In Fig. 1 we plot the  $m(M_{\text{bol}})$  data for each series (with  $M_{\text{bol}} = 4.72$  for the Sun). At a given  $M_{\text{bol}} < 8$ , the different models have masses differing by less than 5%. For  $M_{\text{bol}} > 11$  the difference in masses amounts to less than  $0.02 m_{\odot}$ . In the intermediate region ( $8 < M_{\text{bol}} < 11$ ) the models disagree more substantially. For completeness we mention that Burrows et al. (1993) publish models for very low-mass stars ( $m \leq 0.2 m_{\odot}$ ) that are indistinguishable from the Baraffe et al. (1995) models in Fig. 1. We refer the reader to Leggett et al. (1996) for a comparison of the models published by Burrows et al. with other models in the HR diagram.

Below a mass of about  $0.4 m_{\odot}$  stellar structure changes significantly because stars become fully convective and hydrogen associates to H<sub>2</sub> in the outer layers (Copeland et al. 1970; Kroupa, Tout & Gilmore 1990; Baraffe & Chabrier 1996). Increasing the stellar mass we find that near  $0.35 m_{\odot}$  an increase in energy production leads to dissociation of surface H<sub>2</sub> rather than to an increase in luminosity, and the equilibrium structure adjusts accordingly. Suppression of H<sub>2</sub> formation (see Kroupa, Tout & Gilmore 1990) leads to full convection at a significantly lower stellar mass ( $m \approx 0.25 m_{\odot}$ ). This illustrates the importance of H<sub>2</sub> formation for convection. The region in mass around  $0.35 m_{\odot}$  is critical and additional observational mass–luminosity data is indispensable for constraining the theory of low-mass stellar structure. The derivative  $dm/dM_{\text{bol}}$  emphasizes the differences between models and is a potentially powerful diagnostic.

In Fig. 2 we compare mass–luminosity observations with our new and old models and with the empirical  $m(M_V)$  relation derived by Kroupa, Tout & Gilmore (1993). Theoretical  $M_V$  values are estimated from  $M_{\text{bol}}$  following Kroupa, Tout & Gilmore (1990). The agreement of the models with the data can be estimated by computing the chi-squared statistic for  $M_V > 7.0$  (26 data points):  $\chi^2 = 186$  for the old models,  $\chi^2 = 132$  for the Kroupa, Tout & Gilmore (1993) relation and  $\chi^2 = 57$  for the new models. Significant improvement in the  $m(M_V)$  plane is obtained with the new physics. However, in making this comparison, we must be aware that the model  $m(M_V)$  relations are valid for a single-age, single-metallicity stellar population and that they have been computed with the rather uncertain bolometric corrections. The observational data, on the other hand, represent a mixture of Galactic disk stars of different metal abundance and age.

### 3.2 The first derivative of the mass–(absolute magnitude) relation

Returning to the critical region around  $m = 0.35 m_{\odot}$ , we evaluate  $dm/dM_P$  for the old and new stellar models and in different photometric bands for the Kroupa, Tout & Gilmore (1993) relation. Absolute magnitudes in the photometric J-, H- and K-bands are obtained for each mass from the colour–magnitude relations given by equation (1) of Henry & McCarthy (1993). To obtain absolute I-band magnitudes we select a subset of  $M_V$ ,  $V - I$  data from fig. 10 of Monet et al. (1992) which satisfy  $M_V > 3.96 + 3.34(V - I)$ . This eliminates obvious subdwarfs. A linear regression on the data, with each point weighted by its stated error, gives

$$V - I = 0.308 M_V - 1.046, \quad (1)$$

which is very similar to the relation derived by Stobie, Ishida & Peacock (1989)

$$V - I = 0.299 M_V - 0.865. \quad (2)$$

We also derive a cubic weighted least squares relation

$$V - I = 2.696 \times 10^{-3} M_V^3 - 9.857 \times 10^{-2} M_V^2 + 1.433 M_V - 4.949. \quad (3)$$

These three  $V - I, M_V$  relations allow us to estimate the uncertainties associated with the derivative of the colour-magnitude relation which also enters  $dm/dM_P$ . In particular, equation 3 allows for the steepening of the  $M_V(V - I)$  relation near  $V - I = 2.8$  evident in Fig. 3, in which we plot the colour-magnitude data together with the three relations. This steepening results from the changes in stellar structure discussed in Section 1 and has also been discussed by Leggett, Harris & Dahn (1994).

The derivatives of the mass-(absolute magnitude) relations as functions of  $M_V$  are shown in Fig. 4. We also plot  $dm/dM_P$  for the Kroupa, Tout & Gilmore (1993)  $m(M_V)$  relation in the I-, J-, H- and K-bands. The data are tabulated in the appendix (with equation 1 to transform from  $M_V$  to  $M_I$ ). Conversion to  $M_{\text{bol}}$  from  $M_V$  for our empirical relation is made with  $V - I$  from equation 1 and bolometric corrections from equation 6 of Monet et al. (1992).

The minimum in the derivative of the Kroupa, Tout & Gilmore (1993)  $m(M_V)$  relation is pronounced in all photometric bands and agrees in location and amplitude with the observed photometric stellar luminosity functions in the V- and I-bands. This is no surprise in the V-band because it was derived to maximize the agreement with the observational  $m(M_V)$  data provided by Popper (1980), and that the amplitude and position of the maximum in  $-dm/dM_V$  fit the stellar luminosity function. The luminosity function used here is the estimated parent distribution of Malmquist corrected photometric luminosity functions derived by Kroupa (1995b). This is based on estimates of stellar space densities by photometric parallax from low-spatial resolution but deep pencil-beam surveys. It measures the spatial densities of stellar systems, approximately half of which are binary stars, and thus underestimates the number of faint stars (Buser & Kaeser 1985, Kroupa, Tout & Gilmore 1991, 1993; Piskunov & Malkov 1991; Kroupa 1995a). However the position of the peak in the luminosity function does not change significantly as a result of this bias (fig. 20 in Kroupa, Tout & Gilmore 1993; fig. 1 in Kroupa 1995a). We therefore use the photometric luminosity function, which is based on 448 stars and is statistically much more well defined than the nearby luminosity function, to constrain the *position* and approximate *amplitude* of the minimum in the first derivative of the mass-magnitude relation. We cannot completely constrain the shape of the minimum because this would require detailed knowledge of the stellar mass function. By using these average colour-magnitude relations together with the empirical  $m(M_V)$  relation we are in effect modelling a single metallicity and single age stellar population. This is logically consistent with the adoption of the Malmquist corrected data for the photometric luminosity function because the stellar samples used to define the relationships and the luminosity functions all belong to the solar neighbourhood.

Returning to Fig. 4, we see that the stellar models imply a minimum in  $dm/dM_P$  which approximately agrees in location and amplitude with the maximum in the observed luminosity functions. This is evidence that the peak in the stellar luminosity function is caused by the minimum in  $dm/dM_P$  rather than a maximum in the stellar mass function. However the new stellar models place the peak at an absolute V-band magnitude which is too bright by about 0.8 mag, while the old models were in better agreement with the data.

We first consider changing the two free parameters of stellar evolution: hydrogen abundance  $X$  (or equivalently helium,  $Y$ ) and the ratio  $\alpha$  of the mixing length to the pressure scale height. So as not to be hindered by uncertainties in the  $M_{\text{bol}} - M_V$  relation, we compare the models in bolometric magnitudes and take the best estimate for the photometric luminosity function in bolometric magnitudes obtained by Kroupa (1995b) as the observational data. We use  $M_{\text{bol}} = -2.5 \log_{10}(L/L_\odot) + 4.72$ , where  $L$  is the stellar luminosity. From Fig. 5 we deduce that varying  $\alpha$  with fixed  $X$  has a negligible effect, while varying  $X$  with fixed  $\alpha$  increases the maximum in  $-dm/dM_{\text{bol}}$  for models with more hydrogen and moves it to slightly brighter magnitudes. Reasonable variation in  $\alpha$  and  $X$  cannot bring the maximum in  $-dm/dM_P$  for our (improved) models into agreement with the observations. Thus, although the new models have an improved

chi-squared fit w.r.t. the new mass–(absolute magnitude) data, the location of the minimum in the derivative is too bright by about 0.8 mag in the V-band and about 0.5 mag in  $M_{\text{bol}}$ .

To understand why this is, we compare our stellar models with those of Baraffe et al. (1995) and D’Antona & Mazzitelli (1994). We evaluate  $M_{\text{bol}}$  and fit cubic splines to their  $10^9$  yr isochrones. Derivatives  $dm/dM_{\text{bol}}$  are calculated from the fitted cubic-spline relations and we plot them in Fig. 6. We make the following observations: **(a)** our new models and those of D’Antona & Mazzitelli (1994) place the minimum in  $dm/dM_{\text{bol}}$  at about the same  $M_{\text{bol}} \approx 9$ ; **(b)** the peak in our models is more pronounced; we attribute this to our finer resolution in the mass grid; **(c)** our old models have the minimum at  $M_{\text{bol}} \approx 9.5$ , in agreement with the observations, as already noted above; and **(d)** the most modern stellar models computed by Baraffe et al. (1995) better reproduce the location of the maximum in the luminosity function; the amplitude we derive for their models is again limited by the low resolution of their mass grid.

We find it unlikely that structure would exist in the mass function so close to the point where similar structure would result directly from the mass–luminosity relation. The results of this section and section 4 lend credence to the simplest hypothesis that the peak in the luminosity function results from the maximum in  $-dm/dM_P$ . This hypothesis was basic to the investigation reported in Kroupa, Tout & Gilmore (1990) and used in subsequent work. A mass function with a maximum is also inconsistent with star-count data (Section 9 in Kroupa, Tout & Gilmore 1993). Thus we conclude that fortuitous cancellation of errors in stellar structure led to good agreement between our old models and data. It is only when both interior and atmospheric physics are improved (Baraffe et al. 1995) that we can improve on this fit.

### 3.3 The Hertzsprung-Russel diagram

We have compared stellar models with observations in the mass–luminosity plane and invoked the first derivative of the mass–(absolute magnitude) relation as an additional constraint. We now extend the comparison to the luminosity–(effective temperature) plane. Fig. 7 is the HR diagram for low-mass stars. We take our data from Popper (1980) and Kirkpatrick et al. (1993). The latter describe how their estimates of the effective temperature are hotter than previous empirical estimates by about 300 K for  $M_{\text{bol}} \approx 9.7$  ( $m \approx 0.3 m_{\odot}$ ) and by about 350 K at  $M_{\text{bol}} \approx 12.2$  ( $m \approx 0.1 m_{\odot}$ ). Unfortunately no independent (i.e. from binary star orbits) stellar mass estimates are available for the data published by Kirkpatrick et al. (1993) and we believe they are now superseded by a new empirical determination of  $L(T_{\text{eff}})$  data by Leggett et al. (1996). These data, for Galactic-disc stars, are in good agreement with those of Popper (1980), lying only about 100 K cooler for  $-2.6 < \log_{10}(L/L_{\odot}) < -1.9$ .

All stellar models suggest that the effective temperature increases more slowly with increasing luminosity in the range  $3.46 < \log_{10}(T_{\text{eff}}/\text{K}) < 3.60$ . This is due to the dissociation of  $\text{H}_2$  as  $T_{\text{eff}}$  increases and the related establishment of a radiative stellar core in stars more massive than about  $0.35 m_{\odot}$  and is associated with the minimum in  $dm/dM_P$ . Models of D’Antona & Mazzitelli (1994) are in agreement with the Kirkpatrick et al. (1993) data. Our new models also agree with this data down to about  $0.2 m_{\odot}$  but are too cool at lower masses. However, the models computed by Baraffe et al. (1995) using the most realistic treatment of the atmosphere are too cool by  $\log_{10}T_{\text{eff}} \approx 0.04$  with respect to the Kirkpatrick et al. data, but are in agreement with the older data published by Popper (1980) and the most recent compilation by Leggett et al. (1996). In the  $M_V, V - I$  diagram (figs 1 and 2 in Baraffe et al. 1995) their models are bluer (i.e. hotter) than observational data. Baraffe et al. (1995) discuss the reasons for this.

### 3.4 Summary

We summarise our comparison of stellar models with observed data in Table 1.

**Table 1:** Comparison with observational data

model	$m(M_V)$	HR diagram	$-dm/dM_{\text{bol}}$
our old	OK	too hot for $\log_{10}T_{\text{eff}} < 3.52$	OK
our new	OK	too hot for $3.52 < \log_{10}T_{\text{eff}} < 3.58$	too bright
D'Antona	OK	too hot for $\log_{10}T_{\text{eff}} < 3.58$	too bright
Baraffe	OK	OK	OK

Column 1 lists the models (see Section 2) and column 2 lists our assessment of their fit to the  $m(M_V)$  data plotted in Fig. 2 (see also Fig. 1). Column 3 is our assessment of the fit to the luminosity–(effective temperature) data of Leggett et al. (1996) and Popper (1980). Consistency with the locations of the maximum in  $-dm/dM_{\text{bol}}$  and of the peak in the stellar luminosity function from Kroupa (1995b) is described in column 4.

We conclude that the most sophisticated models by Baraffe et al. (1995) provide the overall best agreement with all recent observational constraints. The same conclusion concerning the HR diagram is also arrived at by Leggett et al. (1996). All models provide reasonable fits to the  $m(M_V)$  data which, without further mass determinations around  $0.35 m_\odot$ , is not sufficient to distinguish between models.

#### 4 IMPLICATIONS FOR LUMINOSITY FUNCTIONS OF POPULATION II STARS

Until recently there were essentially no observational constraints on metal-poor stellar models. Comparison with colour–magnitude data is hindered by our ignorance of the state of the stellar atmosphere. An example is to be found in figs 1 and 2 of Baraffe et al. (1995), where we see that for  $M_V > 15$  the population I models are too blue by up to  $\Delta(V - I) \approx 0.4$ , or conversely, are too bright by  $\Delta M_V \approx 1$  mag for  $V - I > 3.4$ . The population II models, however, appear to fit the subdwarf sequence.

We have demonstrated (Section 3.2) that the location of the minimum in  $dm/dM_P$  can be used as a constraint on stellar models. We can also apply this test to population II stars by comparing the position of the theoretical minimum in the derivative of the mass–magnitude relation with the magnitude of the turnover in observed stellar luminosity functions. Testing metal-poor luminosity functions is also an important step towards establishing whether the mass function varies with star-formation conditions. The behaviour of the location of the turnover in the luminosity function with metallicity is conveniently summarised and extended to Galactic clusters with solar abundance by von Hippel et al. (1996). In their fig. 5 they show how the position of the turnover moves to brighter magnitudes for more metal deficient stellar populations. They compare this with the constant mass locus of stellar models and find acceptable agreement. This suggests that the change in location of the structure in the stellar luminosity function with metallicity may be due to changes in stellar physics rather than the stellar mass function. By considering constant mass loci alone we cannot however establish that the location of the minimum in the derivative of the mass–magnitude relation also behaves like the observational sample. In order to test this in a more consistent way we compare empirical data with the theoretical position of the minimum in  $dm/dM_{\text{bol}}$ .

## 4.1 Theoretical data

For the theoretical data set we compute new stellar models for metallicities  $Z = 0.03, 0.02, 0.01, 0.004, 0.001, 0.0003$  and  $0.0001$  with hydrogen abundance  $X = 0.76 - 3Z$  and helium abundance  $Y = 0.24 + 2Z$ , and plot some of the first derivatives  $dm/dM_{\text{bol}}$  in Fig. 8. All have maxima in  $-dm/dM_{\text{bol}}$  which are at a brighter magnitude  $M_{\text{bol}}^{\max}$  for lower metal abundance. This effect is less significant near the solar value. For a given mass, metal-poorer stars are brighter and a little smaller. Consequently hydrogen dissociation in the outer layers takes place at slightly but not significantly lower masses. These low metallicity stars are still brighter than their metal rich counterparts, and so the inflexion in the mass–magnitude relation moves to higher luminosities with decreasing metallicity. We plot the resulting  $M_{\text{bol}}^{\max}([\text{Fe}/\text{H}])$  relationship in Fig. 9 with filled circles.

Recall that for solar metallicities our models predict an  $M_{\text{bol}}^{\max}$  that is too bright by about 0.8 mag (Section 3.2). However, as indicated by our modelling shown in Fig. 5, we expect the change in  $M_{\text{bol}}^{\max}$  with  $[\text{Fe}/\text{H}]$  to be more robust to changes in stellar physics than the actual position of the maximum  $M_{\text{bol}}^{\max}$ , because it depends primarily on  $Z$ . Available theoretical work (see tables 1–4 in D’Antona & Mazzitelli 1996) suggests that the bolometric corrections for the I-band do not drastically change with metal abundance so that we do not transform our  $M_{\text{bol}}^{\max}$  values to the I-band. We see that this approximation is sufficient for the present purpose by comparing with theoretical  $M_{\text{I}}^{\max}([\text{Fe}/\text{H}])$  values from D’Antona & Mazzitelli (1996). When we compute our own models we can define an arbitrarily high resolution in the mass grid and metallicity grid. However we are limited by not being able to incorporate a realistic stellar atmosphere. D’Antona & Mazzitelli (1996) have also computed stellar models for different metallicities and from their fig. 7 we obtain  $M_{\text{I}}^{\max}([\text{Fe}/\text{H}])$ . They plot theoretical I-band luminosity functions for a constant mass function and from these we compute  $-dm/dM_{\text{I}}$ . Given the sparse grid in stellar masses and the wide magnitude bins we estimate the likely range for the maximum in  $-dm/dM_{\text{I}}$  from the magnitude bin width and thus obtain lower and upper limits on  $M_{\text{I}}^{\max}([\text{Fe}/\text{H}])$ . These are plotted in Fig. 9 as two sets of open squares. Both limiting curves have been shifted by +0.7 mag because their models also place the minimum at too bright a magnitude (Fig. 6).

## 4.2 Observational data

Good observations of four globular clusters are now available. The stellar luminosity functions extend to the vicinity of the hydrogen-burning mass limit and are defined by a few thousand stars. Three of these luminosity functions show the expected structure: the luminosity function of NGC 6397 ( $[\text{Fe}/\text{H}] = -1.91$ ) has a sharp peak at  $M_{\text{I}}^{\max} = 8.55$  (Paresce et al. 1995); for M15 ( $[\text{Fe}/\text{H}] = -2.26$ ) it has a somewhat broader peak at  $M_{\text{I}}^{\max} = 8.60$  (De Marchi & Paresce 1995a); and for 47 Tuc ( $[\text{Fe}/\text{H}] = -0.65$ ) it has a pronounced peak at  $M_{\text{I}}^{\max} = 8.90$  (De Marchi & Paresce 1995b). However the luminosity function of the dynamically young cluster  $\omega$  Cen ( $[\text{Fe}/\text{H}] = -1.60$ , with a substantial spread of abundances), on the other hand, rises to  $M_{\text{I}} = 8.61$  and remains flat at lower luminosities (Elson et al. 1995). Because this luminosity function does not show a pronounced maximum it merits future investigation.

To these globular clusters we add the Galactic clusters NGC 2420, NGC 2477, Pleiades and Hyades, and the solar neighbourhood sample. The luminosity function of NGC 2477 flattens without a peak in a similar way to that of  $\omega$  Cen. For the solar neighbourhood we use the parent distribution of Malmquist corrected photometric luminosity functions estimated by Kroupa (1995b) from 448 stars within a distance of  $100 - 200$  pc of the Sun. We assign it an average  $[\text{Fe}/\text{H}] = -0.2$  (Edvardsson et al. 1993, Wyse & Gilmore 1995). We have already plotted this luminosity function in the V-band magnitudes (Fig. 4) and in bolometric magnitudes (Fig. 5).

We illustrate the uncertainties in determining  $M_{\text{I}}^{\max}$  owing to magnitude binning by marking the bin-boundary magnitudes that bracket the position of the turnover in Fig. 9. For the solar neighbourhood luminosity function we estimate the likely range of  $M_{\text{I}}^{\max}$  from the bin boundaries in the V-band (Kroupa 1995b) and equation 1 and note that reasonable changes in the  $M_{\text{V}}(V - I)$  relation do not significantly affect the estimated values (Fig. 4). For the two luminosity functions that do not show a pronounced maximum we mark the bright bin boundary before the flattening and indicate the next faint bin boundary by an arrowhead.

We divide the sample into two groups: those which are defined by more than a few hundred stars are shown as thick open circles; those with less are shown as thin open circles. These are NGC 2477 (based on 53 stars) and NGC 2420 (only 19 stars) from von Hippel et al. (1996).

The Pleiades ( $[Fe/H] = +0.03$ ) luminosity function (Hambly, Hawkins & Jameson 1991) has a well defined shape with a maximum, but it is not clear how old the low-mass stars are. The canonical age is about  $7 \times 10^7$  yr, but by studying Li depletion Basri, Marcy & Graham (1996) suggest that it may be  $1.2 \times 10^8$  yr. Using the pre-main sequence evolution tracks in table 7 of D'Antona & Mazzitelli (1994) the former age implies that a star with a mass of  $0.3 m_\odot$  lies above the main sequence by  $\delta M_{\text{bol}} \approx 0.37$  mag and the latter estimate implies  $\delta M_{\text{bol}} \approx 0.14$  mag. The distance modulus is usually taken to be 5.5 mag but Gatewood et al. (1990) measure  $5.9 \pm 0.26$  mag. Further discussion of the possible uncertainties is given in section 6.2.1 of Kroupa (1995c). In Fig. 9 we portray these uncertainties by plotting  $M_I^{\max}$  as thin open circles for the various combinations of age and distance modulus.

The Hyades data point is taken from the estimate by Reid (1993) of the luminosity function based on stars with a membership probability of at least 50 per cent (panel a of his fig.8). For the transformation from the V-band to the I-band we use the  $M_V(V - I)$  relationship derived by Reid for the Hyades stars because the cluster is relatively metal rich ( $[Fe/H] = +0.15$ ).

Dynamical evolution of clusters may affect the peak magnitude because low-mass stars preferentially evaporate as a cluster evolves. However the predicted value is quite insensitive to reasonable changes in a power-law mass function (fig. 4 of Kroupa & Gilmore 1994). Figs. 10 and 12 of Kroupa (1995c) show that as a cluster loses low-mass stars to near exhaustion, the peak in the stellar luminosity function moves to a brighter magnitude by only about 0.5 mag in  $M_V$  or 0.29 mag in  $M_{\text{bol}}$ . Because this is smaller than the difference between the high- and low-metallicity clusters plotted in Fig. 9, and because we do not expect any of these clusters to have lost all of their low-mass stars, dynamical evolution does not affect our conclusions.

### 4.3 Interpretation

While the observational sample has large uncertainties, the difference between the high metallicity luminosity functions (Galactic-disc photometric luminosity function, Hyades, Pleiades, NGC 2420, NGC 2477) and the three low-metallicity clusters (M 15,  $\omega$  Cen, NGC 6397) confirms that there is a correlation of peak magnitude with metallicity (Fig. 9). Stellar populations with higher metal abundances tend to have a maximum or turnover in the stellar luminosity function that lies at fainter absolute magnitudes.

Comparison of our theoretical  $dM_{\text{bol}}^{\max}/d[Fe/H]$  relationship with  $dM_I^{\max}/d[Fe/H]$  from D'Antona & Mazzitelli (1996) shows that both are in agreement and also shows that the bolometric corrections for the I-band do not change significantly with metallicity. We do not have to shift our relationship to fainter magnitudes because the bolometric corrections and our offset (Fig. 6) are such that  $M_{\text{bol}}^{\max}([Fe/H])$  coincides roughly with the I-band observational relationship. The observed trend is consistent with the hypothesis that the structure in stellar luminosity functions near  $m = 0.35 m_\odot$  reflects structure in the first derivative of the mass–absolute-magnitude relation and not in the mass function.

## 5 CONCLUSIONS

All the models we have tested are in good individual agreement with data in the mass–luminosity plane (Figs. 1 and 2). The largest differences between models occur near a mass of  $0.35 m_\odot$ , where, as the mass falls, stellar structure changes significantly owing to the onset of full convection and formation of H<sub>2</sub> near the surface. Additional observational mass–luminosity data are required around this critical mass in order to better constrain models. These constraints need not only come from well-determined binary-star orbits but may also be derived from gravitational microlensing of distant stars by high-proper motion (i.e. nearby) stars (Paczynski 1995). The theoretical and empirical HR diagram reflects the changes in stellar interiors at the critical mass (Fig. 7)

Following Kroupa, Tout & Gilmore (1990), we argue that the peak in the stellar luminosity function at  $M_V \approx 11.5$  ( $m \approx 0.35 m_\odot$ ) for population I stars results from the minimum in  $dm/dM_P$ . This gives us an additional constraint on stellar models because the position of the peak is not significantly dependent on the precise slope of a smooth mass function. According to our hypothesis, precise models should have a

maximum in  $-dm/dM_{\text{bol}}$  at  $M_{\text{bol}} \approx 9.8$ . The models computed by Baraffe et al. (1995), who treat the stellar atmosphere in the most detail, are able to reproduce the location of this feature in the stellar luminosity function.

In Section 4 we computed population II stars and found that the minimum in the first derivative of the mass-magnitude relation moves to brighter magnitudes with decreasing metallicity. Our stellar models for metallicity extending down to  $[\text{Fe}/\text{H}] = -2.3$  reproduce the behaviour of the position of the peaks and turnovers of the empirical stellar luminosity functions relative to solar metallicity (Fig. 9). In this way the position of the peak observed in stellar luminosity functions for both metal poor and metal rich stars can be accounted for by the minimum in the first derivative of the mass-(absolute magnitude) relation (see also von Hippel et al. 1996). There is no indication that additional variation of the stellar mass function is needed, but more conclusive results must await a deeper analysis of each individual cluster luminosity function.

Despite the recent significant progress in modelling the internal structure of low-mass stars significant errors remain when a realistic atmosphere is not included: models with a standard Eddington approximation for the surface boundary condition (our models) and those that use a grey atmosphere (D'Antona & Mazzitelli 1994) are both in reasonable agreement with mass-luminosity data but place the maximum in  $-dm/dM_P$  at too bright a magnitude and are too hot for  $\log_{10}(L/L_{\odot}) < -1.4$ . A realistic atmosphere (Baraffe et al. 1995) leads to much better agreement with mass-luminosity data, the estimated maximum in  $-dm/dM_P$  and the luminosity-(effective temperature) data for faint stars.

We urge researchers who can compute stellar models with realistic stellar atmospheres to produce models on a fine grid of masses in the range  $0.1 - 1.0 m_{\odot}$  so as to resolve the extremum in the first derivative of the mass-magnitude relation near a mass of  $0.35 m_{\odot}$ . They should also consider a large range of metallicities so that their models may be tested against an observational sample similar to the one presented in Fig. 9.

## ACKNOWLEDGEMENTS

We thank F. D'Antona for sending us results of her model calculations, and Derek Jones for useful suggestions. We also acknowledge the comments of an anonymous referee. CAT is very grateful to the UK PPARC for an Advanced Fellowship during which much of this work was completed. PK thanks the Institute of Astronomy, Cambridge and the Space Telescope Science Institute, where most of this work was done, for hospitality.

## REFERENCES

- Alexander D.R., Ferguson J.W., 1994, ApJ, 437, 879  
 Anders E., Grevesse N., 1989, Geochim. Cosmochim. Acta, 53, 197  
 Andersen J., 1991, A&AR, 3, 91  
 Baraffe I., Chabrier G., 1996, ApJ, 461, L51  
 Baraffe I., Chabrier G., Allard F., Hauschildt P.H., 1995, ApJ, 446, L35  
 Basri G., Marcy G. W., Graham J. R., 1996, ApJ, 458, 600  
 Burrows A., Hubbard W.B., Saumon D., Lunine J.I., 1993, ApJ, 406, 158  
 Buser R., KAESER U., 1985, A&A, 145, 1  
 Caughlan G.R., Fowler W.A., 1988, At. Data Nucl. Data Tables, 40, 284  
 Caughlan G.R., Fowler W.A., Zimmermann B.A., 1975, ARA&A, 13, 69  
 Chabrier G., Baraffe I., Plez B., 1996, ApJ, 459, L91  
 Copeland H., Jensen J.O., Jorgensen H.E., 1970, A&A, 5, 12  
 Cox A.N., Stewart J.N., 1970, ApJS, 19, 243  
 D'Antona F., Mazzitelli I., 1983, A&A, 127, 149  
 D'Antona F., Mazzitelli I., 1994, ApJS, 90, 467  
 D'Antona F., Mazzitelli I., 1996, ApJ, 456, 329  
 De Marchi G., Paresce F., 1995a, A&A, 304, 202  
 De Marchi G., Paresce F., 1995b, A&A, 304, 211  
 Edvardsson B., Andersen J., Gustafsson B., Lambert D. L., Nissen P. E., Tomkin J., 1993, A&A, 275, 101  
 Eggleton P.P., 1971, MNRAS, 151, 351  
 Eggleton P.P., 1972, MNRAS, 156, 361  
 Eggleton P.P., 1973, MNRAS, 163, 279  
 Eggleton P.P., Faulkner J., Flannery B.P., 1973, A&A, 23, 325  
 Elson R.A.W., Gilmore G.F., Santiago B.X., Casertano S., 1995, AJ, 110, 682  
 Gatewood G., Castelaz M., Han I., Persinger T., Stein J., Stephensen B., Tangren W., 1990, ApJ, 364, 114  
 Hamby N.C., Hawkins M.R.S., Jameson R.F., 1991, MNRAS, 253, 1  
 Henry T.J., McCarthy D.W., 1993, AJ, 106, 773  
 von Hippel T., Gilmore G., Tanvir N., Robinson D., Jones D.H.P., 1996, AJ, 112, 192  
 Hjellming, 1989, PhD thesis, University of Illinois  
 Iglesias C.A., Rogers F.J., Wilson B.G., 1992, ApJ, 397, 717 (OPAL)  
 Kirkpatrick J.D., Kelly D.M., Rieke G.H., Liebert J., Allard F., Wehrse R., 1993, ApJ, 402, 643  
 Kroupa P., 1995a, ApJ 453, 358  
 Kroupa P., 1995b, ApJ 453, 350  
 Kroupa P., 1995c, MNRAS, 277, 1522  
 Kroupa P., Gilmore G., 1994, MNRAS, 269, 655  
 Kroupa P., Tout C.A., Gilmore G., 1990, MNRAS, 244, 76  
 Kroupa P., Tout C.A., Gilmore G., 1991, MNRAS, 251, 293  
 Kroupa P., Tout C.A., Gilmore G., 1993, MNRAS, 262, 545  
 Kurucz R.L., 1991, in Crivellari L., Hubeny I., Hummer D.G., eds, NATO ASI Ser., Stellar Atmospheres: Beyond the Classical Models. Kluwer, Dordrecht, p.441  
 Leggett S. K., Harris H. C., Dahn C. C., 1994, AJ, 108, 944  
 Leggett S. K., Allard F., Berriman G., Dahn C. C., Hauschildt P. H., 1996, ApJS, 104, 117  
 Monet D.G., Dahn C.C., Vrba F.J., Harris H.C., Pier J.R., Luginbuhl C.B., Ables H.D., 1992, AJ, 103, 638  
 Paczyński B., 1995, Acta Astronomica 45, 345  
 Paresce F., De Marchi G., Romaniello M., 1995, ApJ, 440, 216  
 Piskunov A.E., Malkov O.Yu., 1991, A&A, 247, 87  
 Pols O.R., Tout C.A., Eggleton P.P., Han Z., 1995, MNRAS, 274, 964  
 Popper D.M., 1980, ARA&A, 18, 115  
 Reid N., 1993, MNRAS, 265, 785  
 Stobie R.S., Ishida K., Peacock J.A., 1989, MNRAS, 238, 709  
 Tout C.A., Pols O.R., Eggleton P.P., Han Z., 1996, MNRAS, 281, 257

Webbink R.F., 1975, PhD thesis, University of Cambridge

Woolley R.v.d.R., Stibbs D.W.N., 1953. The Outer Layers of a Star. Clarendon Press, Oxford

Wyse R. F. G., Gilmore G., 1995, AJ, 110, 2771

### Figure captions

**Figure 1.** Mass–(absolute bolometric magnitude) relations for solar-abundance stellar models. The solid curve represents our new stellar models and the dashed curve our old models. The models of D'Antona & Mazzitelli (1994) are plotted as the open circles and those of Baraffe et al. (1995) as filled squares

**Figure 2.** Comparison of our new (long-dashed curve) and old (short-dashed curve) solar-abundance stellar models with observations with estimated errors (Henry & McCarthy 1993: open circles; Andersen 1991: open squares). The solid curve is the empirical  $m(M_V)$  relation derived by Kroupa, Tout & Gilmore (1993).

**Figure 3.** Colour–magnitude data from fig. 10 in Monet et al. (1992). Obvious subdwarfs are plotted with asterisks. Dwarfs are shown as errorbars (see Section 3.2 for details). The solid line is our linear regression (equation 1), the long-dashed line is equation (2) (from Stobie et al. 1989) and the short-dashed curve is our cubic fit (equation 3). The dotted line,  $M_V = 3.96 + 3.34(V - I)$ , separates subdwarfs from dwarfs.

**Figure 4.** Derivatives of  $m(M_P)$  relations.

(a) The visual band  $P = V$ . The solid curve is the derivative of the Kroupa, Tout & Gilmore (1993) empirical relation. It peaks at  $M_V = 11.6$ . The long-dashed curve is the derivative of our new models and the short-dashed curve that of our old models. Filled circles are derived from observed luminosity functions (Kroupa 1995b) and scaled to this figure.

(b) The I-band. The three curves are all derivatives of the empirical Kroupa, Tout & Gilmore (1993) relation transformed from the V-band: for the solid curve we used our linear fit (equation 1); for the dotted curve we used Stobie et al. (1889) linear fit (equation 2); and for the dashed curve we used our cubic fit (equation 3). The peak is at  $M_I = 9.00$  irrespective of which relation is used. Open squares are scaled from the luminosity function of the Pleiades (Hambly et al. 1991) with a distance modulus of 6.

(c) The derivatives of the empirical relation in the K (solid line), J (dashed line) and H (dotted line) bands. The peaks are at  $M_K^{\max} = 6.95$ ,  $M_J^{\max} = 7.75$  and  $M_H^{\max} = 7.20$ .

**Figure 5.** The effects of the mixing length ratio  $\alpha$  and hydrogen abundance  $X$  on  $dm/dM_{\text{bol}}$ . The solid line is standard with  $\alpha = 2$  and  $X = 0.7$ . The dashed curve has  $\alpha = 1$  ( $X = 0.7$ ) and the dotted curve has  $X = 0.8$  ( $\alpha = 2$ ). The histogram is the best estimate photometric luminosity function from Kroupa (1995b) which is scaled to fit the figure.

**Figure 6.** Comparison of the first derivative of different theoretical  $m(M_{\text{bol}})$  relations: D'Antona & Mazzitelli (1994), dotted curve; Baraffe et al. (1995), long-dashed curve; our new models, solid line; and old models, short-dashed line. The low-resolution histogram is the photometric luminosity function estimated by Kroupa (1995b) and scaled to fit the figure. The Kroupa, Tout & Gilmore (1993) empirical  $m(M_{\text{bol}})$  relation (Table A) is plotted as a histogram with higher resolution.

**Figure 7.** The Hertzsprung-Russell diagram for low-mass stars. The observational data compiled by Popper (1980) are represented by open symbols corresponding to the masses given in the legend. The empirical estimates of Leggett et al. (1996) are in good agreement with the Popper (1980) data. The data published by Kirkpatrick et al. (1993) are shown by filled circles. Various lines illustrate the stellar models. Transverse dotted lines separate their mass ranges (from bottom to top:  $0.1, 0.2, 0.4, 0.6$  and  $1.0 m_{\odot}$ ).

**Figure 8.** The first derivative of the theoretical  $m(M_{\text{bol}})$  relation for metal abundances  $Z = 0.02$  (solid line),  $Z = 0.01$  (long-dashed line),  $Z = 0.001$  (dash-dotted line),  $Z = 0.0003$  (short-dashed line) and  $Z = 0.0001$  (dotted line).

**Figure 9.** The relative position of the minimum in the first derivative of the  $m(M_I)$  relation as a function of metallicity. The solid circles are the bolometric magnitudes of our models shown in Fig. 8. The open squares connected by dotted lines bracket the position of the maximum in the theoretical  $-dm/dM_I(M_I)$  relations

computed by D'Antona & Mazzitelli (1996) after shifting the maxima by +0.7 mag to account for the offset of the peak from the empirical position (see Fig.6). Each open circle represents the absolute I-band magnitude of the peak or turn-over in the observed luminosity functions of different stellar clusters. Errorbars indicate the bin-width in magnitudes used to construct the luminosity function. Thick symbols represent stellar luminosity functions based on more than a few hundred stars and thin symbols show luminosity functions that are less well defined. The solar-neighbourhood photometric luminosity function is labeled by "SN". The position of the Pleiades luminosity function is shown from top to bottom after adjustment for the following combinations of (distance modulus, age): (5.5,  $7 \times 10^7$  yr), (5.5,  $1.2 \times 10^8$  yr), (5.5, main sequence), (6,  $7 \times 10^7$  yr), (6,  $1.2 \times 10^8$  yr), (6, main sequence).